ACS OMEGA

Open Access

http://pubs.acs.org/journal/acsodf

Article

Structure–Property Relationships of Near-Infrared Cyanine Dyes: Chalcogen-Driven Singlet Oxygen Generation with High Fluorescence Efficiency

Shufan Yang, Ewan Forsyth, Wuyang Lin, Kerry Setchfield, Rachel Crespo-Otero, Devis Di Tommaso, Annamaria Lilienkampf, Amanda Wright, and Mark Bradley*

Cite This: *ACS Omega* 2026, 11, 4475–4484

Read Online

ACCESS | Metrics & More | Article Recommendations | Supporting Information

ABSTRACT: We report the design, synthesis, and optical characterisations of eight novel near-infrared (NIR) cyanine dyes incorporating different chalcogens (O, S, and Se). These dyes exhibited excellent deep-NIR absorption (λ_{max} = 767−833 nm) and emission (λ_{max} = 784−859 nm) profiles. TDDFT calculations matched well the experimental trends and data. All compounds exhibited high extinction coefficients (178,000−267,000 cm^{-1} M^{-1}) and good fluorescence quantum yields, resulting in high overall brightnesses. Remarkably, the selenium-containing dyes featuring terminal indole and benzoindole-type units exhibited impressive singlet oxygen quantum yields of around 13%, a standout performance in the deep-NIR region. These values are particularly promising and highlights the potential of these dyes for deep-NIR imaging and photodynamic applications.

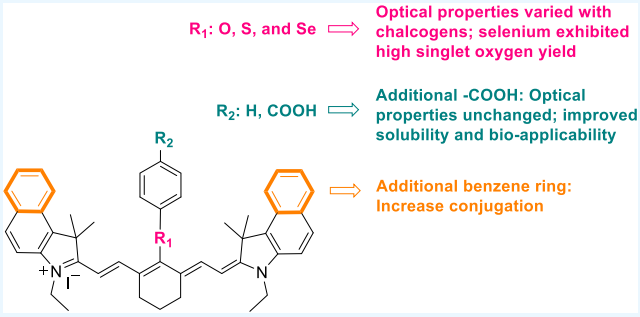

INTRODUCTION

Near-infrared-II (NIR-II) and short-wave infrared (SW-IR) fluorescent imaging have emerged as powerful techniques with broad potential in biological and medical applications.[1−5] This spectral range is advantageous for biological imaging due to reduced light scattering by tissue at these longer wavelengths, and minimal autofluorescence from biological tissues, allowing deeper tissue penetration.[6−8] Indeed, 'Deep-NIR cyanine dyes" (those with wavelengths greater than 750 nm) are prominent in this area, offering enhanced signal-to-noise ratios and improved depth penetration, making them attractive for a range of biomedical applications.[9] There is also increasing demand for deep-NIR dyes that can also generate singlet oxygen - key for photodynamic therapy (PDT).[10−14] PDT is a minimally invasive therapeutic approach that uses light-activated photosensitizers to produce cytotoxic reactive oxygen species, offering spatial and temporal control of treatment, killing when and where illumination occurs.[15] The combination of imaging and therapeutic capabilities offers significant appliction and future promise for the treatment of cancer and other localized diseases.[16]

The broad biocompatibility, tunable photophysical properties and ease of chemical modification of the cyanine dyes has driven their utility. These dyes can be tailored, such as by the addition of solubilizing groups via sulfonylation, or the attachment of ammonium groups or PEG's, or the provision of chemical handles to allow the attachment of ligands enabling the targeted imaging of specific tissues/cells/receptors.[17−19] Of specific note is Indocyanine Green (ICG), a FDA-approved, near-infrared (NIR) fluorescent dye, that is widley used for medical diagnostics, such as measurement of cardiac output and liver function assessment.[20,21] It absorbs (784 nm) and emits in the deep NIR (807 nm) allowing for deep tissue imaging, making it valuable in cancer diagnostics and surgery guidance.[22,23]

Many NIR cyanine dyes that have been reported.[24] For example NIR-780, which is hydrophobic, shows preferential accumulation in tumors, which is useful for both imaging and so-called photothermal therapy (conversion of NIR light into heat to destroy cancer cells).[25,26] NIR-783 is a commercial NIR heptamethine cyanine dye carrying a chemically reactive chloro-group on a cyclohexenyl ring (similar in function to the cell tracker dyes) and has been reported to be selective for imaging various cancer types, including breast and brain, perhaps via covalent albumin conjugation.[27,28] The ability of NIR-783 to preferentially accumulate in tumor cells has been reported to enable both precise imaging and photothermal therapy.[19] Structurally related is the more hydrophobic NIR-786, that also complexes to proteins such as albumin. It has been found to

Received: October 8, 2025
Revised: December 31, 2025
Accepted: January 5, 2026
Published: January 12, 2026

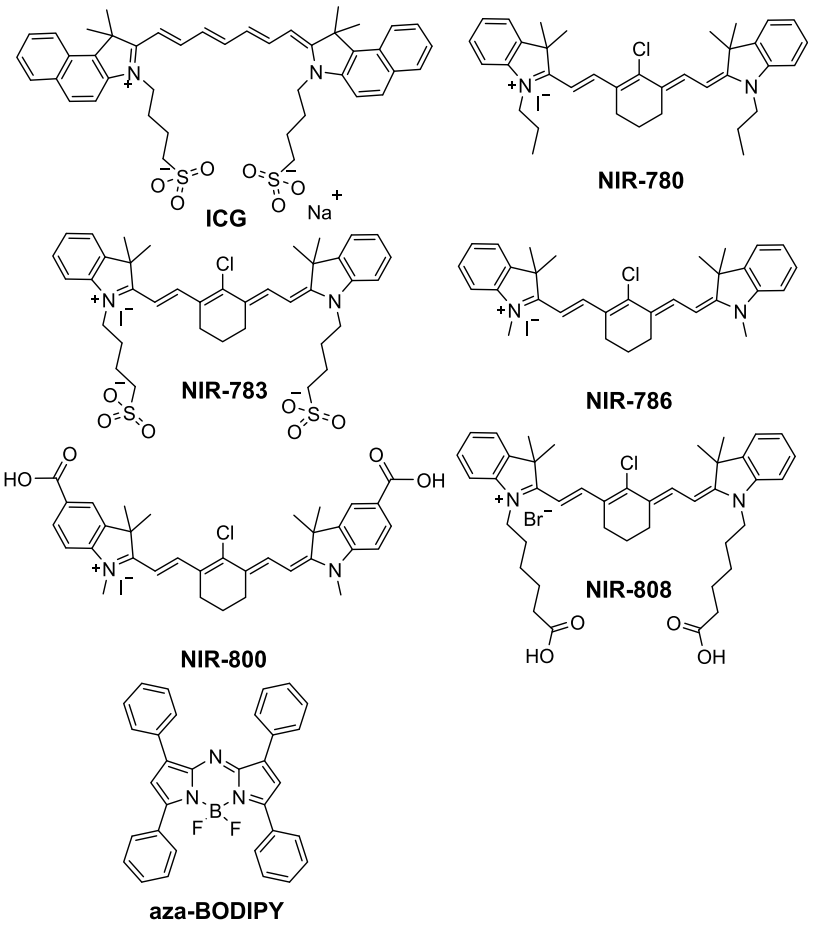

Figure 1. Chemical structures of ICG, NIR-780, NIR-783, NIR-786, NIR-808, NIR-800 and tetraphenyl substituted aza-BODIPY (with a formal zwitterionic structure).

show tumor accumulation, making it effective in photothermal cancer treatment.[24] Also in this family are CA-800Cl (here named NIR-800 to be consistent) and NIR-808 (also referred to as MHI-148),[24] that exhibit similar optical properties, both with the incorporation of two carboxylic acid moieties. The later (NIR-808) has been applied in optical imaging, benefiting from its inherent tumor-targeting ability (via organic anion transporters) without requiring conjugation to targeting peptides.[29]

Recent studies have reported the synthesis of dual-modal imaging agents that combine NIR-II cyanine dyes with magnetic resonance imaging (MRI) contrast agents, offering a more comprehensive tool for tumor detection and surgical navigation.[30,31] Polymer-conjugated cyanine dyes have also been reported, with cyanine dyes attached to biodegradable polymers to improve their circulation time in the bloodstream, making them more effective for long-term imaging and targeted delivery applications.[32,33]

Therefore, given their significant potential, new NIR cyanine dyes occupy an important position and yet still require development to promote chemical/photostability and the ability to offer therapeutic efficacy in the form of photodynamic therapy.[34]

A significant area of research within the realm of dyes/fluorophores involves the design and synthesis of dyes incorporating group 14 elements (beyond carbon) (crystallogens), group 15 elements (pnictogens), and group 16 elements (chalcogens). For example, Koide et al., explored how the integration of Group 14 elements (silicon, germanium, or tin) into rhodamine dyes changed their optical properties.[35] By replacing oxygen atoms in traditional rhodamines with these elements, the dyes exhibited a red-shift in fluorescence emission, moving them into the near-infrared (NIR) range. As for group 15 elements (pnictogens), nitrogen is frequently incorporated into NIR dyes (in place of carbon), such as aza-BODIPY (Figure 1) and aminocyanines.[36,37] Aza-BODIPY dye (Figure 1) exhibits strong absorption in the NIR region (λ_{abs} = 650 nm) following the introduction of additional nitrogen atoms into the linking backbone.[36,37] These modifications shifting the absorption spectra toward longer wavelengths, enhances their flexibility for deep tissue imaging.[37] Other group 15 elements are much less commonly incorporated e.g phosphorus or arsenic due to chemistry challenges and toxicity concerns, although, Adams et al., introduced a method for the fluorescent labeling of proteins with a Cys-Cys-Xaa-Xaa-Cys-Cys motif, binding so-called FlAsH (fluorescein with two As(III) substituents).[38]

In terms of group 16 (chalcogens), oxygen, sulfur, and selenium, can significantly influence the electronic structure and, consequently, the optical properties of the dyes.[39] For example, replacing oxygen with sulfur or selenium can lead to red-shifted absorption and emission wavelengths, altered quantum yields, and changes in photostabilities.[40−42] Liu et al. demonstrated this by modifying heptamethine cyanine dyes with sulphur or selenium, modifying the two indole (indol-1-ium) rings with thiazoles or selenazoles. The *bis*-seleno variant showed a strong redshift (~840 nm) and a highly efficient singlet oxygen generation.[12] Understanding the structure−property relation-

https://doi.org/10.1021/acsomega.5c10499
ACS Omega 2026, 11, 4475−4484

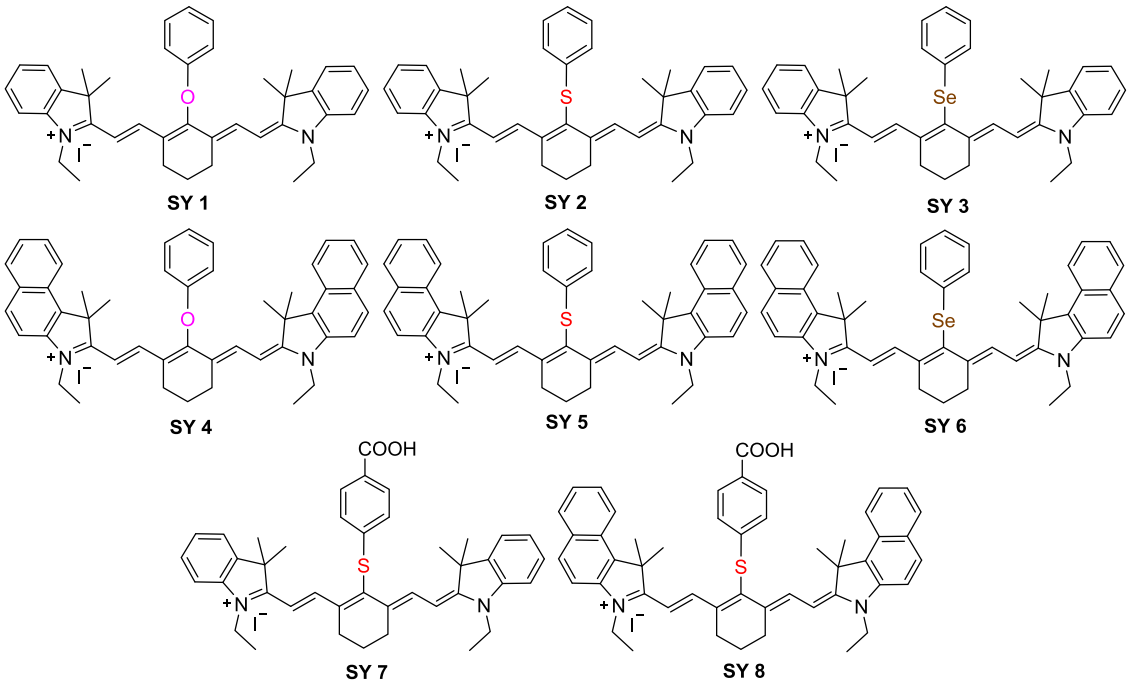

Figure 2. Chemical structures of the synthesized cyanine dyes **SY 1**−**SY 8**.

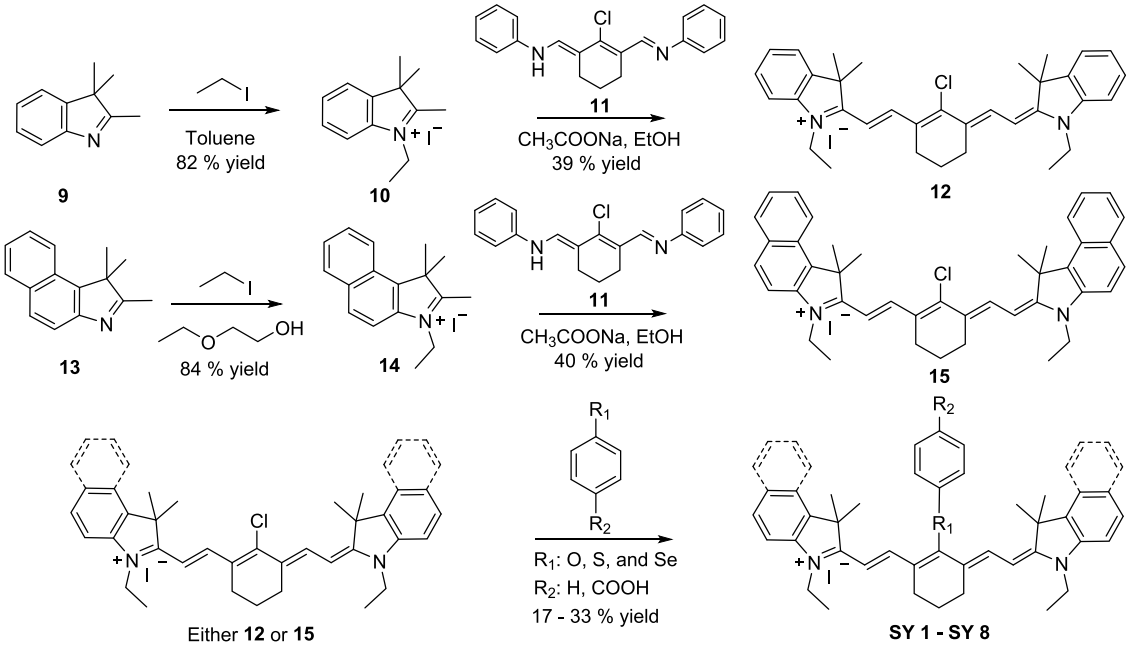

Figure 3. Synthetic route to the 'deep-NIR" fluorophores and singlet oxygen generators **SY 1**−**SY 8**.

ships of these chalcogen-containing dyes and their biological sensitivity and compatibility is important for biological application.

Here we explored the design and synthesis of novel near-infrared cyanine dyes with various chalcogens (O, S, and Se), examining their optical properties and structure−property relationships as well as their ability to generate reactive oxygen species. Increased conjugation at the terminal group altered the optical properties, causing a red shift in the spectrum. We also successfully introduced a −COOH group to some dyes, which preserved the optical properties while enhancing solubility and potential biological applicability. Density functional theory (DFT) and Time-dependent density functional theory (TDDFT) calculations were employed to investigate the optical properties of the chalcogen-containing dyes, showing good agreement with experimental results and supporting the observed trends. This manuscript highlights the potential of these dyes for photodynamic therapy-based applications, with significant levels of singlet oxygen generation by the NIR seleno-variants., which also proved to be remarkably stable to singlet oxygen generation, despite the known propensity of selenium to undergo facile oxidation.

https://doi.org/10.1021/acsomega.5c10499
ACS Omega 2026, 11, 4475−4484

RESULT AND DISCUSSION

The dyes **SY 1**−**SY 8** were synthesized in three steps via N-alkylation of the "indole" or "benzoindole" terminating groups, *bis*-Knoevenagel condensation with the bifunctional core 2-chloro-1-methyl-3-methylenecyclohex-1-ene **11** and nucleophilic displacement of the "reactive" halogen (see Figure 3). They were readily prepared on-scale and purified. The benzoindole derivatives were expected to allow red-shifted absorptions/emissions compared to the indole variants. The nucleophiles were all chalcogen-based (phenol, thiophenol or selenophenol (benzeneselenol)) and gave the cyanine dyes **SY 1**−**SY 6** as green solids, while **SY 7** and **SY 8** were generated using 4-mercaptobenzoic acid, with the carboxylic acid group, enhancing their water-solubility. Due to their varying electronegativities and sizes (O: 3.44, 63 pm S: 2.58, 103 pm Se: 2.54, 116 pm), the chalcogen would be expected to alter the electronic distribution/conjugation and affect the optical properties of the dyes (Figures 2 and 3).

The purified dyes were examined optically with the optical properties varying with the indole/benzoindole head groups and the chalcogen (see Figure 4). With the same chalcogen the absorption spectrum red-shifted when using the different terminal indoles or benzoindoles (as expected). Thus, comparing **SY 1** to **SY 4**, the $\lambda_{max,abs}$ increased from 767 to 805 nm; **SY 2** and **SY 5** increased from 793 to 833 nm; and there was an increase from 787 to 826 nm for **SY 3** and **SY 6**.

When the chalcogen was altered there were subtle changes in the absorption spectrum. In the indole series, from **SY 1** (O) to **SY 2** (S), there was a 26 nm red-shift observed, potentially due to improved conjugation and the reduced electron-withdrawing nature of the central ring. However, the change from **SY 2** (S) to **SY 3** (Se), was observed to result in a very slight blue-shift (793 to 787 nm). Selenium, being a little larger than sulfur and slightly less electronegative, potentially gives rise to this by slightly reducing conjugation across the system or forcing it out of planarity. Similarly, within the benzoindole series, there was a red-shift from 805 to 833 nm when comparing **SY 4** (O) and **SY 5** (S), and a slight blue shift between **SY 5** (S) and **SY 6** (Se) (833 nm decreasing to 826 nm).

Fluorescence emission studies showed that **SY 1** (O) had a $\lambda_{max,em}$ of 784 nm and **SY 4** (O) (the benzoindole variant) had a $\lambda_{max,em}$ of 823 nm, both showing a 17 nm Stokes shift. **SY 3** (Se) had a $\lambda_{max,em}$ of 812 nm with a Stokes shift of 25 nm, while **SY 6** (Se) with its increased conjugation has a $\lambda_{max,em}$ of 854 nm (and a 28 nm Stokes shift). The dyes with the carboxylic acid groups (**SY 7** and **SY 8**) showed identical optical properties as the unmodified dyes (**SY 2** and **SY 5**).

The quantum yields (Φ_F) of **SY 1**−**SY 8** ranged from 6 to 18%, with the benzoindole variants exhibiting a slightly lower Φ_F than the indole variants. The quantum yield values decreased from O > S > Se among both the indole series (**SY 1**−**SY 3**) and the benzoindole series (**SY 4**−**SY 6**) with values of 18, 13, and 11% and 14, 7, and 6% respectively. **SY 7** and **SY 8** had similar quantum yield to **SY 2** and **SY 5**.

Table 1 gives the summary of absorption, fluorescence and Stokes shift data, as well as their extinction coefficients, fluorescence quantum yields, brightness and singlet oxygen quantum yields for the 8 dyes. It is worthwhile to note that all dyes exhibit high molar extinction coefficients ranging from 178,000 to 267,000 cm^{-1} M^{-1}, which along with their fluorescence quantum yields (between 6−18%), resulted in high brightness values between 10,700 and 47,800. There was no quenching observed, even at 5 μM, suggesting the absence of any aggregation effects.

The singlet oxygen quantum yield efficiencies (Φ_{SO}) of **SY 1**−**SY 8** were measured by monitoring the changes in absorbance of 1,3-diphenylisobenzofuran at 410 nm when exposed to the NIR dyes under irradiation (see SI Figure 2). Table 1 gives the singlet oxygen quantum yield efficiencies which ranged from 1 to 13%, much higher than ICG (with a Φ_{SO} of approximately 0.9%),[43] although having a similar cyanine conjugation system. There was no significant change observed in Φ_{SO} between dyes in the indole or benzoindole series with the same chalcogen. Incorporation of Se in dyes **SY 3** and **SY 6** increased singlet oxygen quantum efficiencies (12 and 13% respectively see Figure 5) when compared with their oxygen **SY 1** and **SY 4** (both 5%),[44] and sulfur counterparts **SY 2** (1%) and **SY 5** (2%).[12,45] **SY 7** and **SY 8** exhibited similar Φ_{SO} as **SY 2** and **SY 5** (2 and 3%).

SY 3 and **SY 6** which both contain the chalcogen selenium, benefit from longer excitation wavelengths (>810 nm) and showed the highest singlet oxygen generation efficiencies of all the dyes (approximately 13%).[46−48] Analysis (HPLC) showed that the seleno-dyes remained unchanged during extended irradiation (as do their absorbances as shown in Figure 5),

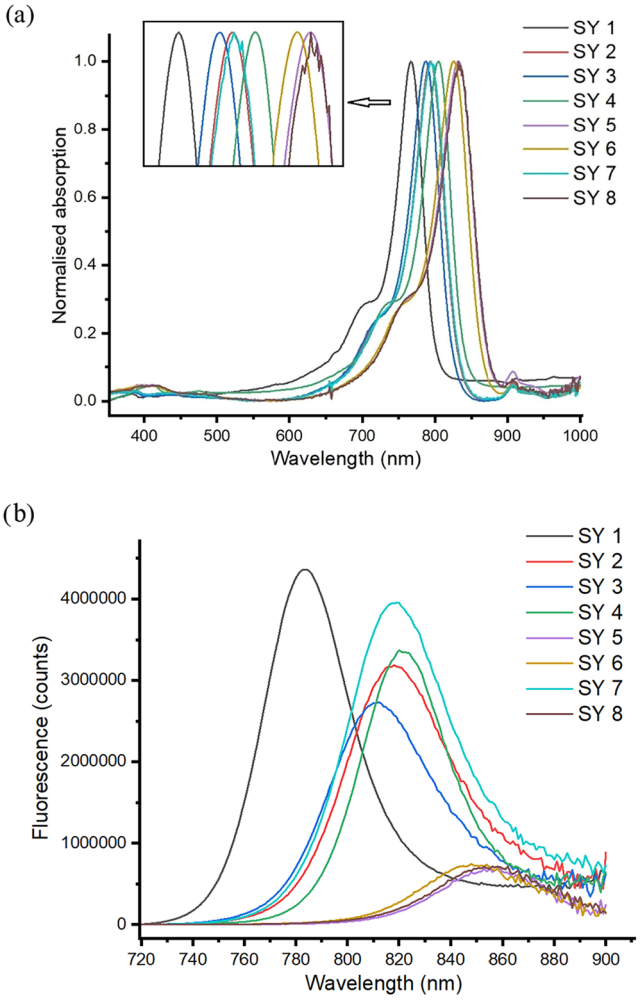

Figure 4. Optical properties of the dyes **SY 1**−**8**. (a) Normalized absorption spectra of the eight NIR dyes (**SY 1**−**SY 8**); (b) Fluorescence spectrum of the dyes **SY 1**−**8**. All the dyes were 2 μM in ethanol with excitation at 710 nm.

https://doi.org/10.1021/acsomega.5c10499
ACS Omega 2026, 11, 4475−4484

Table 1. Extinction coefficients (ε) of each dye were measured from three concentrations (1.25 μM, 2.5 μM and 5 μM). Fluorescence quantum yield measurements of SY 1 − SY 8 were carried out in ethanol (2 μM); Indocyanine Green in ethanol (ICG, Φ = 13.2 %) was used as the reference for fluorescence quantum yield measurements.[49] The singlet oxygen quantum yields were measured using Methylene blue in MeOH ($\Phi\Delta$ = 52 %) as a reference, with each dye evaluated at 5 μM in MeOH.[50]

Dye	Structure	$\lambda_{max,\ abs}$ (nm)	$\lambda_{max,\ em}$ (nm)	Stokes shift (nm)	Stokes shift (cm^{-1})	ε $cm^{-1}M^{-1}$	Φ_F	Brightness	Φ_{SO}
SY 1	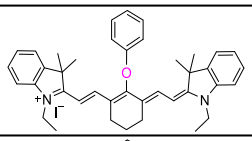	767	784	17	282	266000	18 %	47800	5 %
SY 2	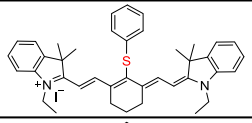	793	818	25	385	216000	13 %	28000	1 %
SY 3	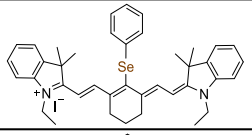	787	812	25	391	199000	11 %	21900	12 %
SY 4	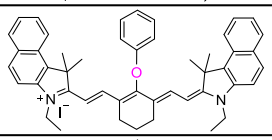	805	823	18	271	267000	14 %	37400	5 %
SY 5	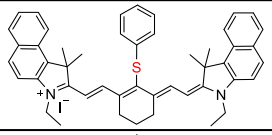	833	859	26	363	246000	7 %	17200	2 %
SY 6	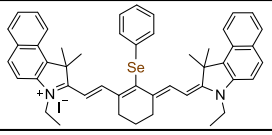	826	854	28	397	178000	6 %	10700	13 %
SY 7	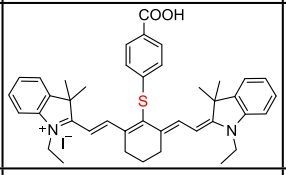	794	819	25	384	204000	11 %	22400	2 %
SY 8	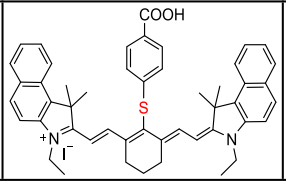	832	858	26	364	274000	7 %	19000	3 %

confounding fears of selenium oxidation by the photogenerated singlet oxygen. The calculated S_1-T_1 gap for all the dyes **SY 1**−**SY 6** were approximately 0.8 eV, indicating an energetically accessible intersystem crossing (ISC) pathway, and supporting the proposed singlet oxygen generation mechanism (Table S9).

THEORETICAL INVESTIGATIONS

To explore the absorption and fluorescence emission processes/properties, density functional theory (DFT) and time-dependent density functional theory (TD-DFT) calculations were performed on the dyes **SY 1**−**SY 8** (for details see the SI Section). The optimized structures of **SY 1**−**SY 8**, along with the corresponding HOMO and LUMO orbital contours, are shown in Figure 6. In the indole series, the oxygen-containing dye **SY 1** had the largest gap (2.04 eV), while the S-containing dye **SY 2** (1.95 eV) showed a similar gap to the Se-containing dye **SY 3** (1.93 eV). The largest gap for **SY 1** may originate from the more electronegative character of O, which leads to higher electronic localization. The energy gaps decreased with the reduction in electronegativity from O to S, to Se. The benzoindole series exhibited a smaller HOMO−LUMO gap compared to the indole counterpart, with the different chalcogens exhibiting a similar trend to that observed in the previous series. The calculated gaps were 1.95 eV for **SY 4** (O), and 1.88 eV for SY **5** (S) and **SY 6** (Se). The additional ring in the benzoindoles series enhancing the delocalization of electrons. The carboxylic group did not cause any noticeable differences in the HOMO−LUMO gap. These excitation energies accurately reproduce the experimentally observed λ_{max} values across the indole and benzoindole series with the different chalcogens (Table 2).

https://doi.org/10.1021/acsomega.5c10499
ACS Omega 2026, 11, 4475−4484

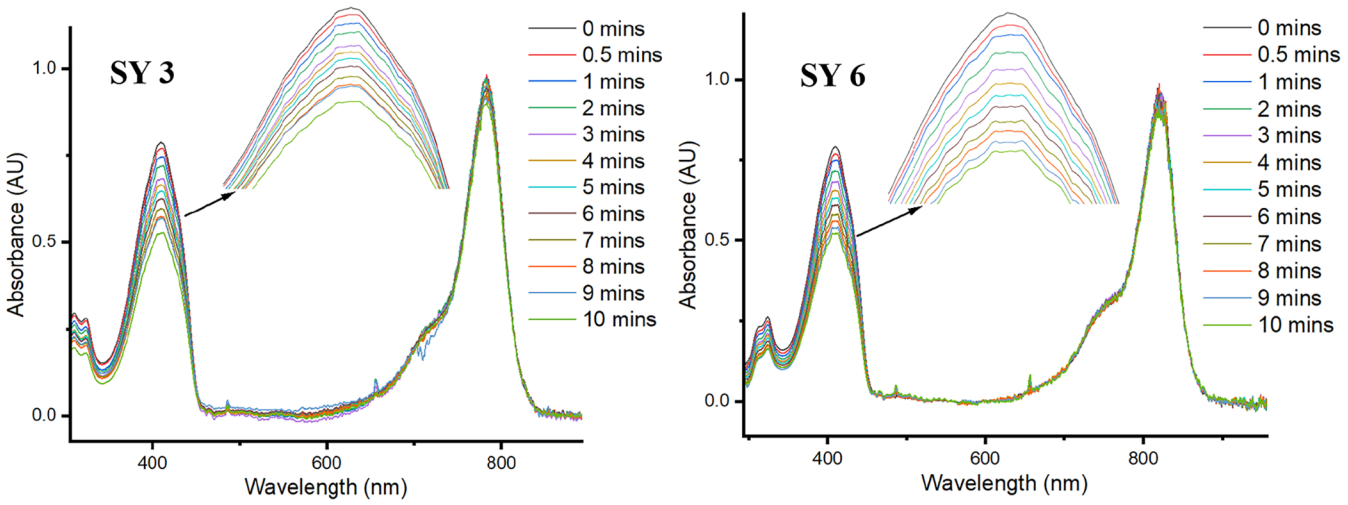

Figure 5. Singlet oxygen generation by **SY 3** and **SY 6**. Change of absorbance with time for DPBF (50 μM) in MeOH treated with **SY 3** and **SY 6** (5 μM) upon irradiation (lamp power 0.02 W/cm^2, long pass filter > 490 nm).

The TD-DFT values for fluorescence energies and emission wavelengths further support the experimental results. Calculations conducted on the first excited state were used to analyze the fluorescence emission process, and determined the energy gaps of 1.64, 1.49, and 1.51 eV for the three indole dyes (**SY 1**−**SY 3**) and 1.48, 1.45, and 1.46 eV for the three benzoindole dyes (**SY 4**−**SY 6**). Similar to the absorption process, the additional carboxylic acid group has little impact on the fluorescence emission. Our computational results suggest that O-containing dyes displayed the largest energy gap in both absorption and fluorescence emission processes, followed by Se- and S-containing dyes, while the indole series displayed larger gaps than the benzoindoles. The attached carboxylic acid group exerted barely any effect on the properties of these dyes. Given the inverse relationship between the energy gaps and emission spectrum, these results agree well with our experimental results, specifically, the blue shift caused by the O and the red shift caused by S in the same series.

EXPERIMENTAL SECTION

The Synthesis of SY 1

The synthesis of **SY 1** followed the synthetic procedure of Wang.[51] **12** (80 mg, 0.125 mmol) and phenol (117 mg, 1.25 mmol) were dissolved in DMF (5 mL), and triethylamine (0.1 mL) was added. The reaction mixture was stirred under an N_2 atmosphere for 24 h at room temperature. After the reaction was complete (shown by TLC), the solvent was removed in vacuo and the residue purified by column chromatography on silica gel (eluting with dichloromethane: ethanol = 100:1 to 20:1), yielding the title compound **SY 1** as a green solid (23 mg, 26%). **^{1}H NMR** (400 MHz, $CDCl_3$) δ 7.87 (d, 2H, J = 14.2 Hz), 7.35−7.29 (m, 4H), 7.21 (d, 2H, J = 6.7 Hz), 7.14 (t, 2H, J = 7.4 Hz), 7.09 (d, 2H, J = 8.0 Hz), 7.02 (d, 2H, J = 7.9 Hz), 6.98 (apparent t, 1H, J = 7.4 Hz), 6.02 (d, 2H, J = 14.2 Hz), 4.12 (q, 4H, J = 7.2 Hz), 2.71 (apparent t, 4H, J = 6.0 Hz), 2.05−1.99 (m, 2H), 1.37 (t, 6H, J = 7.2 Hz), 1.28 (s, 12H). **^{13}C NMR** (100 MHz, $CDCl_3$) δ 171.4, 164.1, 159.7, 142.2, 141.7, 141.1, 130.3, 128.7, 125.0, 122.5, 122.4, 122.1, 114.5, 110.5, 99.7, 48.9, 39.8, 27.8, 24.6, 21.1, 12.4. **HRMS** (ES m/z): $[M]^+$ calc. for $C_{40}H_{45}N_2O_1$: 569.35264, found: 569.3514.

The Synthesis of SY 2

12 (80 mg, 0.108 mmol) and thiophenol (36 mg, 0.324 mmol) were dissolved in degassed DMF (10 mL). The reaction was stirred until **12** had been consumed (TLC analysis). DMF was removed under *vacuum* at 50 °C, and the residue was washed with diethyl ether. The solid was purified by column chromatography on silica gel (eluting with dichloromethane: acetone = 100:1 to 4:1) to yield the green title compound **SY 2** (26 mg, 33%). **^{1}H NMR** (400 MHz, $CDCl_3$) δ 8.68 (d, 2H, J = 14.2 Hz), 7.35 (td, 2H, J = 1.2 Hz, J = 7.9 Hz), 7.29−7.26 (m, 2H), 7.25−7.23 (m, 2H), 7.20−7.17 (m, 4H), 7.13 (d, 2H, J = 8.0 Hz), 7.09−7.04 (m, 1H), 6.21 (d, 2H, J = 14.1 Hz), 4.20 (q, 4H, J = 7.2 Hz), 2.79 (apparent t, 4H, J = 6.1 Hz), 2.07−2.01 (m, 2H), 1.46 (s, 12H), 1.42 (t, 6H, J = 7.2 Hz); **^{13}C NMR** (100 MHz, $CDCl_3$) δ 171.9, 151.5, 146.3, 141.8, 141.3, 137.3, 134.3, 129.6, 128.8, 126.1, 125.8, 125.3, 122.3, 110.7, 101.4, 49.3, 40.1, 27.9, 26.9, 20.9, 12.6. **HRMS** (ES m/z): $[M]^+$ calc. for $C_{40}H_{45}N_2S_1$: 585.32980, found: 585.3311.

The Synthesis of SY 3

12 (80 mg, 0.108 mmol) and 3 equiv of benzeneselenol (52 mg, 0.324 mmol) were stirred in anhydrous DMF (20 mL) under N_2 (ballon). The solution was stirred at room temperature overnight. TLC inspection of the reaction showed **12** had been completely consumed. The DMF was removed under *vacuum* at 50 °C and the resulting crude product was purified by silica gel column chromatography (eluting with DCM/acetone = 30:1) to give the green target compound **SY 3** (22 mg, 27%). **^{1}H NMR** (400 MHz, $CDCl_3$) δ 8.73 (d, 2H, J = 14.1 Hz), 7.35 (td, 2H, J = 1.2 Hz, J = 7.86 Hz), 7.29−7.26 (m, 4H), 7.23−7.16 (m, 4H), 7.14−7.07 (m, 3H), 6.18 (d, 2H, J = 14.1 Hz), 4.19 (q, 4H, J = 7.2 Hz), 2.78 (apparent t, 4H, J = 6.1 Hz), 2.05−1.99 (m, 2H), 1.48 (s, 12H), 1.42 (t, 6H, J = 7.2 Hz); **^{13}C NMR** (100 MHz, $CDCl_3$) δ 171.9, 154.7, 149.4, 141.8, 141.3, 134.7, 132.4, 129.8, 128.8, 128.5, 126.4, 125.2, 122.3, 110.7, 101.2, 49.3, 40.0, 27.8, 27.3, 21.0, 12.5. **HRMS** (ES m/z): $[M]^+$ calc. for $C_{40}H_{45}N_2Se_1$: 633.27425, found: 633.2732.

The Synthesis of SY 4

The synthesis of **SY 4** followed the same procedure as **SY 1**, using **15** (90 mg, 0.121 mmol) and 3 equiv of phenol (35 mg, 0.365 mmol). The crude was purified by silica gel chromatography (eluting with dichloromethane/ethanol = 100:1 to 10:1) to give the title compound **SY 4** as a dark green solid (29 mg, 30% yield) **^{1}H NMR** (400 MHz, $CDCl_3$) δ 8.01−7.95 (m, 4H), 7.90−7.86 (m, 4H), 7.53 (t, 2H, J = 7.2 Hz), 7.42−7.38 (m, 6H), 7.11 (d, 2H, J = 8.3 Hz), 7.03 (apparent t, 1H, J = 7.3 Hz), 6.07 (d, 2H, J = 14.3 Hz), 4.26 (q, 4H, J = 7.1 Hz), 2.81−2.72 (m, 4H), 2.08−2.05 (m, 2H), 1.61 (s, 12H), 1.44 (t, 6H, J = 7.0 Hz); **^{13}C NMR** (100 MHz, $CDCl_3$) δ 172.8, 163.7, 159.8, 141.2, 139.2, 133.8, 131.8, 130.8, 130.4, 130.1, 128.1, 127.7, 124.9, 122.5, 122.2, 122.0, 114.6, 110.6, 99.3, 50.8, 40.1, 27.4, 24.7, 21.2, 12.7. **HRMS** (ES m/z): $[M]^+$ calc. for $C_{48}H_{49}N_2O_1$: 669.38394, found: 669.3837.

The Synthesis of SY 5

The synthesis of **SY 5** followed the same procedure as **SY 2**, using **15** (90 mg, 0.121 mmol) and 3 equiv of thiophenol (40 mg, 0.365 mmol). The crude was purified by column chromatography on silica gel, eluting

https://doi.org/10.1021/acsomega.5c10499
ACS Omega 2026, 11, 4475−4484

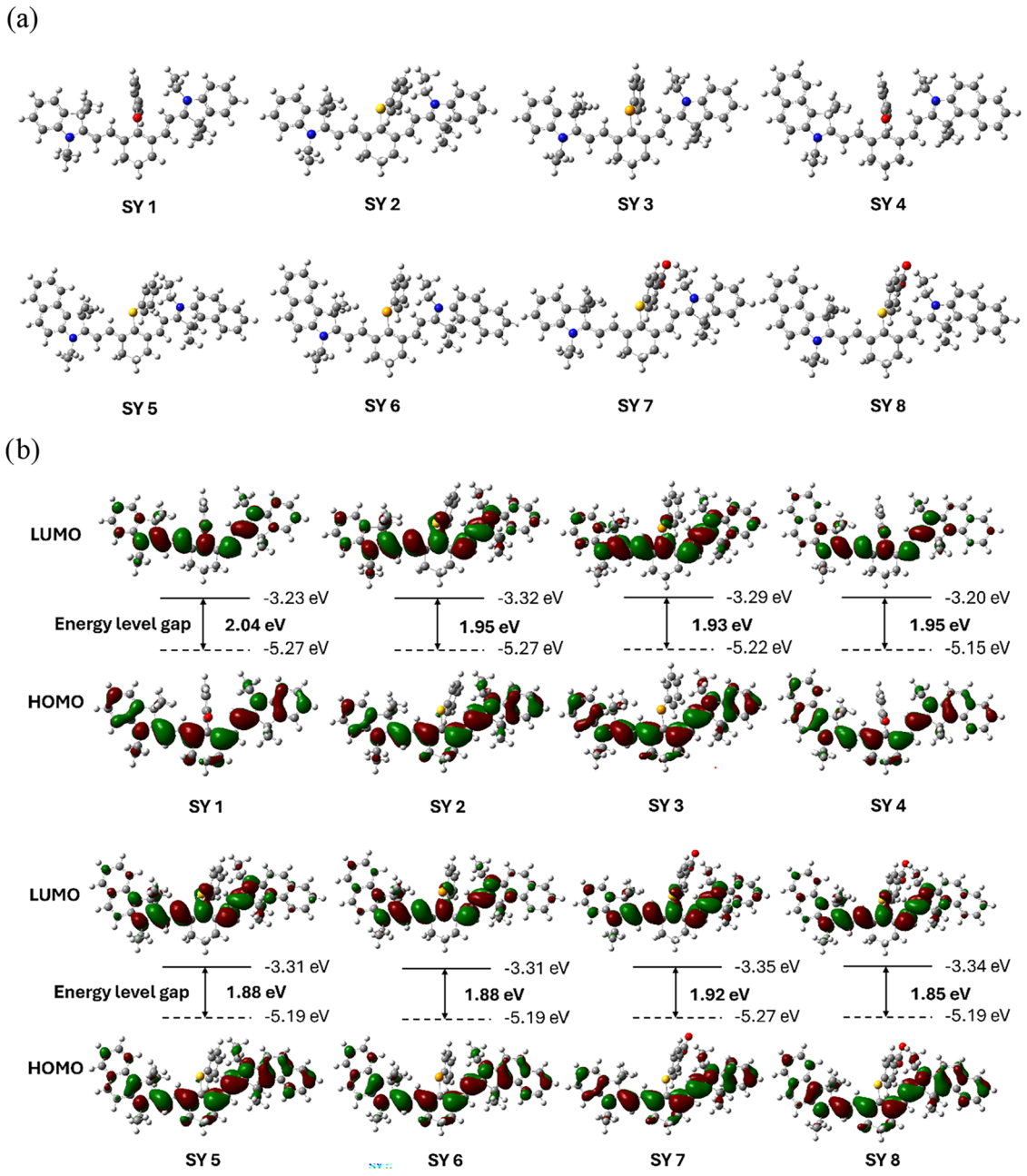

Figure 6. (a) Optimized geometric structures of **SY 1**−**SY 8**, respectively. Gray: carbon, red: oxygen, blue: nitrogen, white: hydrogen, yellow: sulfur and orange: selenium; (b) HOMO and LUMO orbital contours of **SY 1**−**SY 8**.

Table 2. Summary of the results of the energy gap calculations for the absorption and fluorescence emission processes, along with the corresponding spectral peaks for each dye. E_g: HOMO-LUMO energy gap; $E_{abs,cal}$: TD-DFT excitation energy from the S_0 geometry to the first singlet excitation energies. $E_{abs,exp}$: Experimental absorption. $E_{ems,cal}$: TDDFT emission energy from S1 geometry; $E_{ems,exp}$: Experimental emissions; f_{cal}: Calculated oscillator strengths. Values of the energies in eV and of the oscillatory strengths in arbitrary units.

NIR dyes	HOMO (eV)	LUMO (eV)	E_g (eV)	$E_{abs,cal}$ (eV)	$E_{abs,exp}$ (eV)	$E_{ems,cal}$ (eV)	$E_{ems,exp}$ (eV)	f_{cal}
SY 1	−5.27	−3.23	2.04	1.94	1.62	1.64	1.58	2.0293
SY 2	−5.27	−3.32	1.95	1.85	1.56	1.49	1.52	1.8088
SY 3	−5.22	−3.29	1.93	1.87	1.57	1.51	1.53	2.0008
SY 4	−5.15	−3.2	1.95	1.82	1.54	1.48	1.51	2.0758
SY 5	−5.19	−3.31	1.88	1.75	1.48	1.45	1.44	1.9303
SY 6	−5.19	−3.31	1.92	1.76	1.50	1.46	1.45	1.9268
SY 7	−5.27	−3.35	1.92	1.84	1.56	1.48	1.51	1.8735
SY 8	−5.19	−3.34	1.85	1.74	1.49	1.45	1.45	1.9818

https://doi.org/10.1021/acsomega.5c10499
ACS Omega 2026, 11, 4475−4484

with dichloromethane/acetone from 50:1 to 20:1 to yield the title compound **SY 5** (25 mg, 26%) as a dark green solid. **^{1}H NMR** (400 MHz, $CDCl_3$) δ 8.78 (d, 2H, J = 14.2 Hz), 8.02 (d, 2H, J = 8.51 Hz), 7.91−7.87 (m, 4H), 7.56−7.52 (m, 2H), 7.43−7.39 (m, 4H), 7.27−7.24 (m, 4H), 7.08−7.03 (m, 1H), 6.22 (d, 2H, J = 14.2 Hz), 4.31 (q, 4H, J = 7.2 Hz), 2.80 (apparent t, 4H, J = 6.1 Hz), 2.08−2.03 (m, 2H), 1.74 (s, 12H), 1.46 (t, 6H, J = 7.2 Hz); **^{13}C NMR** (100 MHz, $CDCl_3$) δ 173.2, 150.8, 145.3, 139.2, 137.3, 134.0, 133.9, 131.9, 130.8, 130.1, 129.5, 128.1, 127.7, 126.1, 125.7, 125.1, 122.1, 110.7, 100.8, 51.0, 40.3, 31.0, 27.4, 26.8, 12.9. **HRMS** (ES m/z): $[M]^+$ calc. for $C_{48}H_{49}N_2S_1$: 685.36110, found: 685.3582.

The Synthesis of SY 6

The synthesis of **SY 6** followed the same procedure as **SY 3**, using **15** (90 mg, 0.121 mmol) and 3 equiv of benzeneselenol (57 mg, 0.365 mmol). The resulting crude was purified by column chromatography on silica gel, eluting with dichloromethane/acetone from 30:1 to 10:1 to yield the title compound **SY 6** (29 mg, 28%) as a green solid. **^{1}H NMR** (400 MHz, $CDCl_3$) δ 8.86 (d, 2H, J = 14.2 Hz), 8.04 (d, 2H, J = 8.5 Hz), 7.93−7.89 (m, 4H), 7.58−7.54 (m, 2H), 7.45−7.41 (m, 4H), 7.37−7.34 (m, 2H), 7.27−7.23 (m, 2H), 7.13−7.09 (m, 1H), 6.24 (d, 2H, J = 14.2 Hz), 4.33 (q, 4H, J = 7.2 Hz), 2.84 (apparent t, 4H, J = 6.1 Hz), 2.09−2.03 (m, 2H), 1.79 (s, 12H), 1.49 (t, 6H, J = 7.2 Hz); **^{13}C NMR** (100 MHz, $CDCl_3$) δ 173.2, 150.8, 145.3, 139.2, 137.3, 134.0, 133.9, 131.9, 130.8, 130.1, 129.5, 128.1, 127.7, 126.1, 125.7, 125.1, 122.1, 110.7, 100.8, 51.0, 40.3, 31.0, 27.4, 26.8, 12.9. **HRMS** (ES m/z): $[M]^+$ calc. for $C_{48}H_{49}N_2Se_1$: 733.30555, found: 733.3043.

The Synthesis of SY 7

Compound **12** (100 mg, 0.156 mmol) and 4-mercaptobenzoic acid (72 mg, 0.47 mmol) were dissolved in anhydrous DMF (20 mL) under N_2. The solution was stirred at room temperature until TLC inspection showed **12** was completely consumed. The DMF was removed under *vacuum* at 42 °C, and the residue was dissolved in dichloromethane (1 mL) and purified by column chromatography on silica gel (eluting using pure acetone), yielding the pure product **SY 7** as a green solid (23 mg, 19%). **^{1}H NMR** (500 MHz, $CDCl_3$) δ 8.62 (d, 2H, J = 14.1 Hz), 8.00 (d, 2H, J = 8.6 Hz), 7.32 (t, 2H, J = 8.7 Hz), 7.25 (d, 2H, J = 7.5 Hz), 7.18−7.10 (m, 6H), 6.15 (d, 2H, J = 14.1 Hz), 4.15 (q, 4H, J = 7.2 Hz), 2.76−2.74 (m, 4H), 2.03−2.00 (m, 2H), 1.41−1.38 (m, 18H); **^{13}C NMR** (125 MHz, $CDCl_3$) δ 172.1, 169.8, 151.0, 146.3, 141.8, 141.4, 141.1, 134.0, 131.8, 131.2, 128.8, 125.4, 125.2, 122.4, 110.7, 101.3, 49.4, 40.0, 27.9, 26.8, 20.9, 12.6. **HRMS** (ES m/z): $[M]^+$ calc. for $C_{41}H_{45}N_2O_2S_1$: 629.31963, found: 629.3177.

The Synthesis of SY 8

Compound **15** (100 mg, 0.135 mmol) and 4-mercaptobenzoic acid (62 mg, 0.41 mmol) were dissolved in anhydrous DMF (20 mL) under N_2. The resulting solution was stirred at room temperature and stopped when **15** was consumed (TLC analysis). After evaporation of the DMF, the solid residue was extracted with DCM (1 mL), which was evaporated and the crude was purified by column chromatography on silica gel, eluting using dichloromethane/acetone (1:1 to pure acetone), yielding **SY 8** a dark green solid product (25 mg, 21%). **^{1}H NMR** (600 MHz, $CDCl_3$) δ 8.68 (d, 2H, J = 14.1 Hz), 8.00−7.96 (m, 4H), 7.88 (t, 4H, J = 9.0 Hz), 7.53 (t, 2H, J = 8.0 Hz), 7.42−7.39 (m, 4H), 7.32 (d, 2H, J = 8.5 Hz), 6.26 (d, 2H, J = 14.2 Hz), 4.32 (q, 4H, J = 7.2 Hz), 2.87−2.84 (m, 4H), 2.10−2.08 (m, 2H), 1.71 (s, 12H), 1.46 (t, 6H, J = 7.0 Hz); **^{13}C NMR** (125 MHz, $CDCl_3$) δ 173.3, 170.1, 148.3, 144.8, 144.7, 139.2, 134.2, 134.1, 132.0, 131.2, 130.9, 130.2, 128.1, 127.8, 125.6, 125.2, 122.1, 118.1, 110.7, 101.2, 51.1, 40.5, 27.4, 27.0, 20.9, 12.8. **HRMS** (ES m/z): $[M]^+$ calc. for $C_{49}H_{49}N_2O_2S_1$: 729.35093, found: 729.3490.

CONCLUSION

In summary, the design, synthesis, and optical characterisations of a series of eight near-infrared cyanine dyes containing different chalcogens (O, S, and Se) was conducted and their outstanding deep-NIR absorption and emission properties was demonstrated. Compared to the indole series (with $\lambda_{max,\ abs}$/$\lambda_{max,\ ems}$ ranging from 767 to 820 nm), the benzoindole series exhibited a more significant red-shift in both absorption and emission, ranging from 800 nm up to 850 nm. The fluorescence quantum yields ranged from 6% to 18%, with the indole series showing slightly higher quantum yields. TDDFT calculations used to investigate the absorption, emission, and energy gaps of the chalcogen-containing dyes, closely reflected the experimental data, reinforcing the observed photophysical trends. The singlet oxygen quantum yields for the selenium series, **SY 3** and **SY 6**, were both around 13%, high values considering the deep NIR excitation wavelengths were 812 and 854 nm respectively (the excitation energy at 850 nm is 141 kJ/mol, while the singlet oxygen $^1\Delta_g$ state is 95 kJ/mol above the $^3\Sigma_g^-$ ground state). Interestingly, while the change from indole to benzoindole had no observable impact on singlet oxygen generation, the selection of chalcogen did, with the Se-based dyes exhibiting the highest Φ_{SO}, followed by the O and S variants. This is perhaps surprising in view of the propensity of selenium compounds to be readily oxidized, but this dye, with an absorption wavelengths $\lambda_{max,abs}$ of 826 nm and an extinction coefficient of 178,000 cm^{-1} M^{-1}, undergoes rapid singlet oxygen generation upon illumination at low illumination power (0.02 W/cm^2) and in view of their ready synthesis and NIR absorption properties offer potential in photodynamic applications.

ASSOCIATED CONTENT

Supporting Information

The Supporting Information is available free of charge at https://pubs.acs.org/doi/10.1021/acsomega.5c10499.

Computational details including DFT and TDDFT calculations. Singlet oxygen generation studies. Detailed synthetic procedures and characterization data including NMR and HRMS spectra (PDF)

AUTHOR INFORMATION

Corresponding Author

Mark Bradley − *Precision Healthcare University Research Institute, Queen Mary University of London, E1 1HH London, U.K.*; orcid.org/0000-0001-7893-1575; Email: m.bradley@qmul.ac.uk

Authors

Shufan Yang − *School of Chemistry, University of Edinburgh, EH9 3FJ Edinburgh, U.K.; Precision Healthcare University Research Institute, Queen Mary University of London, E1 1HH London, U.K.*; orcid.org/0009-0006-1964-3155

Ewan Forsyth − *Department of Chemistry, University of Oxford, OX1 3TA Oxford, U.K.*; orcid.org/0000-0001-6694-1231

Wuyang Lin − *School of Physical and Chemical Sciences, Queen Mary University of London, London E1 4NS, U.K.*

Kerry Setchfield − *Electrical and Electronic Engineering, University of Nottingham, Nottingham NG7 2RD, U.K.*

Rachel Crespo-Otero − *Department of Chemistry, University College London, London WC1H 0AJ, U.K.*; orcid.org/0000-0002-8725-5350

Devis Di Tommaso − *School of Physical and Chemical Sciences, Queen Mary University of London, London E1 4NS, U.K.; Digital Environment Research Institute, Queen Mary University of London, London E1 1HH, U.K.*; orcid.org/0000-0002-4485-4468

https://doi.org/10.1021/acsomega.5c10499
ACS Omega 2026, 11, 4475−4484

Annamaria Lilienkampf − *School of Chemistry, University of Edinburgh, EH9 3FJ Edinburgh, U.K.;* orcid.org/0000-0002-3593-0393

Amanda Wright − *Electrical and Electronic Engineering, University of Nottingham, Nottingham NG7 2RD, U.K.*

Complete contact information is available at: https://pubs.acs.org/10.1021/acsomega.5c10499

Notes

The authors declare no competing financial interest.

■ ACKNOWLEDGMENTS

We would like to acknowledge funding from the Engineering and Physical Sciences Research Council (EPSRC, United Kingdom) (grant EP/T020997). The computational aspects of this research were carried out using Queen Mary's Apocrita high-performance computing facility, with support from QMUL Research-IT. 10.5281/zenodo.438045.

■ REFERENCES

(1) Hilderbrand, S. A.; Weissleder, R. Near-infrared fluorescence: application to in vivo molecular imaging. *Curr. Opin. Chem. Biol.* **2010**, *14* (1), 71−79.

(2) Liu, P.; Mu, X.; Zhang, X.; Ming, D. The near-infrared-II fluorophores and advanced microscopy technologies development and application in bioimaging. *Bioconjugate Chem.* **2020**, *31* (2), 260−275.

(3) Zhang, N.-n.; Lu, C.; Chen, M.; Xu, X.; Shu, G.; Du, Y.; Ji, J. Recent advances in near-infrared II imaging technology for biological detection. *J. Nanobiotechnol.* **2021**, *19* (1), 132.

(4) Wang, S.; Fan, Y.; Li, D.; Sun, C.; Lei, Z.; Lu, L.; Wang, T.; Zhang, F. Anti-quenching NIR-II molecular fluorophores for in vivo high-contrast imaging and pH sensing. *Nat. Commun.* **2019**, *10* (1), No. 1058.

(5) Carr, J. A.; Franke, D.; Caram, J. R.; Perkinson, C. F.; Saif, M.; Askoxylakis, V.; Datta, M.; Fukumura, D.; Jain, R. K.; Bawendi, M. G.; Bruns, O. T. Shortwave infrared fluorescence imaging with the clinically approved near-infrared dye indocyanine green. *Proc. Natl. Acad. Sci. U.S.A.* **2018**, *115* (17), 4465−4470.

(6) Chang, Z.; Liu, F.; Wang, L.; Deng, M.; Zhou, C.; Sun, Q.; Chu, J. Near-infrared dyes, nanomaterials and proteins. *Chin. Chem. Lett.* **2019**, *30* (10), 1856−1882.

(7) Wan, H.; Yue, J.; Zhu, S.; Uno, T.; Zhang, X.; Yang, Q.; Yu, K.; Hong, G.; Wang, J.; Li, L.; Ma, Z.; Gao, H.; Zhong, Y.; Su, J.; Antaris, A. L.; Xia, Y.; Luo, J.; Liang, Y.; Dai, H. A bright organic NIR-II nanofluorophore for three-dimensional imaging into biological tissues. *Nat. Commun.* **2018**, *9* (1), No. 1171.

(8) Lopalco, M.; Koini, E. N.; Cho, J. K.; Bradley, M. Catch and release microwave mediated synthesis of cyanine dyes. *Org. Biomol. Chem.* **2009**, *7* (5), 856−859.

(9) Rehman, S.; Brennan, P. M.; Lilienkampf, A.; Bradley, M. Approved and investigational fluorescent optical imaging agents for disease detection in surgery. *Int. J. Surgery* **2023**, *109* (8), 2378 DOI: 10.1097/JS9.0000000000000459.

(10) Chinna Ayya Swamy, P.; Sivaraman, G.; Priyanka, R. N.; Raja, S. O.; Ponnuvel, K.; Shanmugpriya, J.; Gulyani, A. Near Infrared (NIR) absorbing dyes as promising photosensitizer for photo dynamic therapy. *Coord. Chem. Rev.* **2020**, *411*, No. 213233.

(11) Yang, Y.; Jiang, S.; Stanciu, S. G.; Peng, H.; Wu, A.; Yang, F. Photodynamic therapy with NIR-II probes: review on state-of-the-art tools and strategies. *Materials Horizons* **2024**, *11* (23), 5815−5842.

(12) Liu, W.; He, S.; Ma, X.; Lv, C.; Gu, H.; Cao, J.; Du, J.; Sun, W.; Fan, J.; Peng, X. Near−infrared heptamethine cyanine photosensitizers with efficient singlet oxygen generation for anticancer photodynamic therapy. *Angew. Chem., Int. Ed.* **2024**, *63* (47), No. e202411802.

(13) Peng, L.; Chen, W.; Hou, H.; Tian, M.; Song, F.; Zheng, W.-H.; Peng, X. Red-to-near-infrared self-reporting photosensitizers with high photostability for photodynamic therapy. *Dyes Pigm.* **2023**, *217*, No. 111426.

(14) Ciubini, B.; Visentin, S.; Serpe, L.; Canaparo, R.; Fin, A.; Barbero, N. Design and synthesis of symmetrical pentamethine cyanine dyes as NIR photosensitizers for PDT. *Dyes Pigm.* **2019**, *160*, 806−813.

(15) Zhou, Z.; Song, J.; Nie, L.; Chen, X. Reactive oxygen species generating systems meeting challenges of photodynamic cancer therapy. *Chem. Soc. Rev.* **2016**, *45* (23), 6597−6626.

(16) Nguyen, V.-N.; Yan, Y.; Zhao, J.; Yoon, J. Heavy-Atom-Free Photosensitizers: From Molecular Design to Applications in the Photodynamic Therapy of Cancer. *Acc. Chem. Res.* **2021**, *54* (1), 207−220.

(17) Wang, S.; Li, B.; Zhang, F. Molecular Fluorophores for Deep-Tissue Bioimaging. *ACS Cent. Sci.* **2020**, *6* (8), 1302−1316.

(18) Bai, J.-W.; Qiu, S.-Q.; Zhang, G.-J. Molecular and functional imaging in cancer-targeted therapy: current applications and future directions. *Signal Transduction Targeted Ther.* **2023**, *8* (1), 89.

(19) Park, Y.; Park, M. H.; Hyun, H. Structure-Inherent Tumor-Targeted IR-783 for Near-Infrared Fluorescence-Guided Photothermal Therapy. *Int. J. Molecular Sci.* **2024**, *25*, 5309 DOI: 10.3390/ijms25105309.

(20) Devriendt, N.; Serrano, G.; Paepe, D.; de Rooster, H. Liver function tests in dogs with congenital portosystemic shunts and their potential to determine persistent shunting after surgical attenuation. *Vet. J.* **2020**, *261*, No. 105478.

(21) Vos, J. J.; Wietasch, J. K. G.; Absalom, A. R.; Hendriks, H. G. D.; Scheeren, T. W. L. Green light for liver function monitoring using indocyanine green? An overview of current clinical applications. *Anaesthesia* **2014**, *69* (12), 1364−1376.

(22) Lange, N.; Szlasa, W.; Saczko, J.; Chwiłkowska, A. Potential of cyanine derived dyes in photodynamic therapy. *Pharmaceutics* **2021**, *13* (6), 818.

(23) Fernandez-Fernandez, A.; Manchanda, R.; Lei, T.; Carvajal, D. A.; Tang, Y.; Kazmi, S. Z. R.; McGoron, A. J. Comparative study of the optical and heat generation properties of IR820 and indocyanine green. *Molecular Imaging* **2012**, *11* (2), No. 7290.2011.00031.

(24) Lim, W.; Byun, J. Y.; Jo, G.; Kim, E. J.; Park, M. H.; Hyun, H. Molecular tuning of IR-786 for improved tumor imaging and photothermal therapy. *Pharmaceutics* **2022**, *14* (3), 676.

(25) Zhang, C.; Liu, T.; Su, Y.; Luo, S.; Zhu, Y.; Tan, X.; Fan, S.; Zhang, L.; Zhou, Y.; Cheng, T.; Shi, C. A near-infrared fluorescent heptamethine indocyanine dye with preferential tumor accumulation for in vivo imaging. *Biomaterials* **2010**, *31* (25), 6612−6617.

(26) Luo, S.; Zhang, E.; Su, Y.; Cheng, T.; Shi, C. A review of NIR dyes in cancer targeting and imaging. *Biomaterials* **2011**, *32* (29), 7127−7138.

(27) Usama, S. M.; Lin, C.-M.; Burgess, K. On the mechanisms of uptake of tumor-seeking cyanine dyes. *Bioconjugate Chem.* **2018**, *29* (11), 3886−3895.

(28) Thavornpradit, S.; Usama, S. M.; Park, G. K.; Shrestha, J. P.; Nomura, S.; Baek, Y.; Choi, H. S.; Burgess, K. QuatCy: A heptamethine cyanine modification with improved characteristics. *Theranostics* **2019**, *9* (10), 2856−2867.

(29) Zhang, L.; Jia, H.; Liu, X.; Zou, Y.; Sun, J.; Liu, M.; Jia, S.; Liu, N.; Li, Y.; Wang, Q. Heptamethine cyanine−based application for cancer theranostics. *Front. Pharmacol.* **2022**, *12*, 764654 DOI: 10.3389/fphar.2021.764654.

(30) Du, Y.; Liu, X.; Zhu, S. Near-Infrared-II Cyanine/Polymethine Dyes, Current State and Perspective. *Front. Chem.* **2021**, *9*, 718709 DOI: 10.3389/fchem.2021.718709.

(31) Liu, C.; Chang, Z.; Chen, K.; Xue, Q.; Shu, B.; Wei, Z.; Zhou, X.; Guo, L.; Zhang, Y.; Pan, Y.; Cao, Q.; Liang, H.; Sun, Q.; Zhang, X. A mitochondrion-targeted cyanine agent for NIR-II fluorescence-guided surgery combined with intraoperative photothermal therapy to reduce prostate cancer recurrence. *J. Nanobiotechnol.* **2024**, *22* (1), 224.

(32) Ma, X.; Shi, L.; Zhang, B.; Liu, L.; Fu, Y.; Zhang, X. Recent advances in bioprobes and biolabels based on cyanine dyes. *Anal. Bioanal. Chem.* **2022**, *414* (16), 4551−4573.

(33) Lawrance, R.; Chowdhury, P.; Lin, H.-C.; Chan, Y.-H. The luminous frontier: transformative NIR-IIa fluorescent polymer dots for deep-tissue imaging. *RSC Appl. Polym.* **2024**, *2*, 749−774, DOI: 10.1039/D4LP00076E.
(34) Chen, X.; Li, J.; Roy, S.; Ullah, Z.; Gu, J.; Huang, H.; Yu, C.; Wang, X.; Wang, H.; Zhang, Y.; Guo, B. Development of Polymethine Dyes for NIR-II Fluorescence Imaging and Therapy. *Adv. Healthcare Mater.* **2024**, *13* (16), No. 2304506.
(35) Koide, Y.; Urano, Y.; Hanaoka, K.; Terai, T.; Nagano, T. Evolution of group 14 rhodamines as platforms for near-Infrared fluorescence probes utilizing photoinduced electron transfer. *ACS Chem. Biol.* **2011**, *6* (6), 600−608.
(36) Sharad Rohidas, P.; Amol, S. C. Synthesis and optical properties of near-infrared (NIR) absorbing azo dyes. In *Chemistry and Technology of Natural and Synthetic Dyes and Pigments*; IntechOpen, 2020, Chapter 11.
(37) Kaur, M.; Janaagal, A.; Balsukuri, N.; Gupta, I. Evolution of Aza-BODIPY dyes-A hot topic. *Coord. Chem. Rev.* **2024**, *498*, No. 215428.
(38) Adams, S. R.; Campbell, R. E.; Gross, L. A.; Martin, B. R.; Walkup, G. K.; Yao, Y.; Llopis, J.; Tsien, R. Y. New biarsenical ligands and tetracysteine motifs for protein labeling in vitro and in vivo: synthesis and biological applications. *J. Am. Chem. Soc.* **2002**, *124* (21), 6063−6076.
(39) Chen, K.; Chen, X.; Hu, K.; Zhao, Y.; Liu, Y.; Liu, G.; Chen, J.; Jiang, W.; Shuai, Z.; Qu, D.; Wang, Z. Enhancing the deep-red/near-infrared fluorescence of higher rylene diimides via the chalcogen-annulation strategy. *Sci. China Chem.* **2024**, *67* (4), 1324−1333.
(40) Prejanò, M.; Alberto, M. E.; De Simone, B. C.; Marino, T.; Toscano, M.; Russo, N. Sulphur- and selenium-for-oxygen replacement as a strategy to obtain dual type I/type II photosensitizers for photodynamic therapy. *Molecules* **2023**, *28*, 3153.
(41) Ilina, K.; MacCuaig, W. M.; Laramie, M.; Jeouty, J. N.; McNally, L. R.; Henary, M. Squaraine dyes: molecular design for different applications and remaining challenges. *Bioconjugate Chem.* **2020**, *31* (2), 194−213.
(42) Shen, J.; He, W. The fabrication strategies of near-infrared absorbing transition metal complexes. *Coord. Chem. Rev.* **2023**, *483*, No. 215096.
(43) Ruhi, M. K.; Ak, A.; Gülsoy, M. Dose-dependent photochemical/photothermal toxicity of indocyanine green-based therapy on three different cancer cell lines. *Photodiagn. Photodyn. Ther.* **2018**, *21*, 334−343.
(44) Benson, S.; de Moliner, F.; Fernandez, A.; Kuru, E.; Asiimwe, N. L.; Lee, J.-S.; Hamilton, L.; Sieger, D.; Bravo, I. R.; Elliot, A. M.; Feng, Y.; Vendrell, M. Photoactivatable metabolic warheads enable precise and safe ablation of target cells in vivo. *Nat. Commun.* **2021**, *12* (1), No. 2369.
(45) Santra, M.; Owens, M.; Birch, G.; Bradley, M. Near-infrared-emitting hemicyanines and their photodynamic killing of cancer cells. *ACS Appl. Bio Mater.* **2021**, *4* (12), 8503−8508.
(46) Bonesi, S. M.; Fagnoni, M.; Monti, S.; Albini, A. Reaction of singlet oxygen with some benzylic sulfides. *Tetrahedron* **2006**, *62* (46), 10716−10723.
(47) Legros, J.; Dehli, J. R.; Bolm, C. Applications of catalytic asymmetric sulfide oxidations to the syntheses of biologically active slfoxides. *Adv. Synth. Catal.* **2005**, *347* (1), 19−31.
(48) Zhang, D.; Ye, B.; Ho, D. G.; Gao, R.; Selke, M. Chemistry of singlet oxygen with arylphosphines. *Tetrahedron* **2006**, *62* (46), 10729−10733.
(49) Rurack, K.; Spieles, M. Fluorescence quantum yields of a series of red and near-infrared dyes emitting at 600−1000 nm. *Anal. Chem.* **2011**, *83* (4), 1232−1242.
(50) Usui, Y. Determination of quantum yield of singlet oxygen formation by photosensitization. *Chem. Lett.* **1973**, *2* (7), 743−744.
(51) Wang, X.; Lv, J.; Yao, X.; Li, Y.; Huang, F.; Li, M.; Yang, J.; Ruan, X.; Tang, B. Screening and investigation of a cyanine fluorescent probe for simultaneous sensing of glutathione and cysteine under single excitation. *Chem. Commun.* **2014**, *50* (97), 15439−15442.

https://doi.org/10.1021/acsomega.5c10499
ACS Omega 2026, 11, 4475−4484